RSC Advances

ROYAL SOCIETY OF CHEMISTRY

www.rsc.org/advances

Eco-friendly Synthesis and Photodegradation of Hierarchical Nanostructures β-FeOOH and α-Fe_2O_3

Zan Li, Guoli Meng, Rufen Chen, Xiuqin Song *

(College of Chemistry and Materials Science, Hebei Normal University, Shijiazhuang 050016, China)

*Corresponding Author. Tel: +86 0311 86268016

Email: xiuqinsong@126.com

Abstract: Hierarchical nanostructures β-FeOOH and α-Fe_2O_3 with different morphology were successfully synthesized via a facile and green hydrolysis-aging method using urea or saccharide as organic matrix. Experimental results showed that the well crystallized β-FeOOH and α-Fe_2O_3 could obtain without higher temperature processing. Systematic control on the morphology and microstructure of the products was achieved by regulating the aging time and the concentration of organic matrix. The amount of saccharide was very important in stabilizing metastable β-FeOOH. The formation mechanism of various morphologies and the cause of stabilizing β-FeOOH were tentatively proposed on the basis of the evolution of the structure and the morphology, along with variation of the reactive conditions. Also, degradation efficiencies of the α-Fe_2O_3 and β-FeOOH with different morphologies toward methylene blue were preliminarily investigated, revealing that as-obtained α-Fe_2O_3 and β-FeOOH possessed promising photodegradation activity and had potential application in wastewater treatment.

Keywords: α-Fe_2O_3; β-FeOOH; Hierarchical Nanostructures; Eco-friendly Synthesis; Photodegradation

1. Introduction

In the development of materials, one of the key and challenging strategies is to explore new, easy and general methods for the preparation of hierarchical nanosructured materials as well as for the control of their structures, size, and morphology. It is important not only for their fundamental scientific interest but also for many technological applications. In the literatures, a variety of hierarchical nanostructured iron oxides had been fabricated [1-6]. However, easy and facile method for synthesis hierarchical nanostructures iron oxides is still highly valuable.

Iron oxides, which combine such functionality with low cost, low toxicity and various attractive physical and chemical properties, have been extensively studied in many fields, especially in environment protection [7-14]. Additionally, iron oxides provide an interesting system for the development of models to explain linkages among aggregation, phase transformation and morphology development [15-16].

Hematite (α-Fe_2O_3) is the most stable iron oxide under ambient conditions and also an important n-type semiconductor (Eg = 2.1 eV) [17]. Nanostructured α-Fe_2O_3 have been demonstrated not only excellent photocatalytic activity for water oxidation, degradation of organic pollutants, and antimicrobial, but also effective adsorption ability for organic dyes and heavy metal ions [18-21]. Various approaches have been developed to fabricate various morphological α-Fe_2O_3 nanostructures. These methods include hydrothermal precipitation reaction [9], hydrothermal-wicrowave method [22], solvothermal method [23], microwave-assisted solvothermal method [24], continuous spray pyrolysis method [25], liquid phase-based ultrasonic-assisted method [26], biphasic interfacial reaction [27], thermal decomposition process [28], chemical precipitation reaction [29], biomimetic synthesis [30], and so on.

Akaganeite (β-FeOOH) is also an important kind of iron oxides semiconductor with a band gap of 2.12 eV. Likewise, β-FeOOH has attracted much attention because of its channel-type nanoporous structure and unique sorption, ion exchange, and catalytic properties [31-34]. On other hand, β-FeOOH is always served as a precursor in the preparation of ferromagnetic α-Fe_2O_3 because of its thermodynamic metastable

feature. But it used to require strict means for preparation and require high temperature for processing β-FeOOH to obtain α-Fe_2O_3 [35-37].

In this study, we present a facile, low-temperature, and environmentally friendly process to prepare hierarchical nanostructured α-Fe_2O_3 and β-FeOOH by hydrolysis of ferric chloride. Compared with the previous reports, the advantages of this method include at least the following points: (1) The method is simple and timesaving, which mainly includes the process of the boiling hydrolysis and water bath aging at 90 °C. (2) The reaction condition is mild. Hierarchical nanostructured α-Fe_2O_3 and β-FeOOH with high crystallinity, purity and regular morphology were directly produced under 80 °C drying conditions without calcinations, which can effectively prevent particles grew up and agglomeration. (3) The reaction routes are very clean and friendly to the environment. Formation of productions was accomplished only by the presence of urea or saccharide, which are non – toxic and biocompatible, without addition of any other organic additives, organic solvent and surfactant. (4) The reaction process is controllable. Just aging time or the amount of saccharide controlling, we could obtain the products with certain morphology and phase structure. The main conclusions resulting from this facial method are as follows: (1) The hierarchical nanostructured α-Fe_2O_3 and β-FeOOH can be constituted through aggregation of primary nanoparticles, which have higher stability and regular morphology. (2) The urea exhibits the control action on the crystallization and morphology of iron oxides. (3) The saccharides play an important role in the controlling products morphology and stabilizing β-FeOOH crystalline phase. A possible growth and transformation mechanism of the as-prepared β-FeOOH to α-Fe_2O_3, especially stabilization of β-FeOOH, was tentatively proposed and discussed based on the experimental results. This work not only can develop a simple general method for preparing hierarchical nanostructure iron oxides but also enable us to further understand the control effect of natural organic on the structure and morphology in the formation of iron oxides. So the results can provide theoretical basis for the biomimetic synthesis of iron oxides.

2. Experimental section

2.1 Preparation of iron oxides

Chemicals: Ferric chloride, urea, glucose, starch and methylene blue are all of analytical grade quality. Ganoderan is obtained from Beijing Fuyuankang Biological Technology Co. Ltd. Polystyrene spheres (PS) are obtained from Shijiazhuang resin plant. All the reagents were used without further purification.

Preparation: Products were prepared by three kinds of initial procedures: ① 5mL saturated solution (3.4mol/L) of $FeCl_3$ were added dropwise into 90 mL boiling water to obtain the brown sol. Then 5mL different levels (2.5-30.0mol/L) of urea solutions were added to the above sol system respectively. ② Using glucose (1-80mg/mL) instead of urea. ③ 5mL saturated solution (3.4mol/L) of $FeCl_3$ were added dropwise into 90 mL water-saccharide solution. The different sols were formed and coagulated through above procedures. After coagulation of sol, the reaction systems were transferred to water bath at the temperature of 90 ℃ for aging different time (1-12h). Then the vessel was cooled down to room temperature under atmospheric condition. The whole process of reaction was under vigorous stirring ceaselessly and within the optimum pH range 4 - 5. The precipitates were separated, washed with distilled water and absolute ethanol, and dried at 80 ℃ for 24h to obtained the final desired products. Scheme 1 is a schematic procedure of various technologies of preparation in our work.

2.2 Characterization

An X-ray diffraction (XRD) study was carried out using a Bruker D8 Advance X-ray diffractometer with Cu Ka radiation (λ= 1.5418Å). Scanning electron microscopy (SEM) measurements were performed with a Hitachi S-4800 microscope. Transmission electron microscopy (TEM), high-resolution TEM (HRTEM) images and selected-area electron diffraction (SAED) patterns were recorded on a JEOL, JEM – 2100 transmission electron microscope, using an accelerating voltage of 200 kV. The surface area and porous structure of the samples were analyzed by nitrogen adsorption in a NOVA4000e nitrogen adsorption apparatus. UV-vis measurements

were carried out in a UV-vis spectrophotometer (VIS - 7220).

2.3 Photodegradation activity measurement

The photo-degradation of methylene blue was carried out in an aqueous solution at room temperature under sunlight irradiation. In a typical experiment, 20 mg photo-catalyst were dispersed in 100 mL methylene blue solution (20 mg/L), followed by the addition of 0.1 mL of hydrogen peroxide solution (30 wt%). The suspension was stirred magnetically 0.5h in the dark in order to reach adsorption equilibrium. At the given time intervals, about 5ml of the suspension was taken from the reaction beaker for the analysis of methylene blue concentration after centrifuging. The photo-catalytic activities of the samples were evaluated by measuring the absorbance of methylene blue solution at 664 nm as a function of irradiation time. Every experiment was repeated at least three times, and the average (with RSD less than 5% for three repeated results) was used as the final results. The degradation rate (%) was evaluated by the following equation:

$$D = [(C_0 - C_t)/C_0] \times 100\%$$

Where D is degradation rate, C_0 and C_t are the concentrations of the methylene blue solution at sunlight irradiation time 0 and t, respectively.

To explore the potential applications of obtained hierarchical architectures α-Fe_2O_3 as photo-catalysis, we specifically prepared nano/microstructure α-Fe_2O_3/PS composite particles by adding polystyrene spheres (PS) to boiling water before the preparation process were implemented.

3. Results and discussion

3.1 The effect of urea on the structure and morphology of the products

To illustrate the role of urea in the formation of iron oxide, the reference experiments, under the same conditions and just without adding urea, were first performed. We noted the following phenomena: (1) The colloidal system generated by adding $FeCl_3$ saturated solution to boiling water dropwise was relatively stable and no

any gelatinous precipitate in the same reaction time. (2) When given enough reaction time, structure of the as-obtained precipitates was amorphization and morphology was anomalous. When adding urea, colloidal particles were easily coagulated, but also the as-obtained products had the relative order hierarchical morphology and the definite crystal structures after series of same treatment.

The effects of aging time on the crystal structures of the as-synthesized products while urea existed were firstly investigated and analyzed. Fig. 1a showed the typical XRD pattern of products obtained at vary aging time but similarly by 80 °C drying in the end. As shown in Fig.1a, when aging time was shorter, the reflection peaks could be approximately indexed to a tetragonal β-FeOOH (JCPDS 34-1266). Then tetragonal β-FeOOH transformed into hexagonal α-Fe_2O_3 gradually with aging time. Finally pure hexagonal α-Fe_2O_3 was obtained. All the diffraction peaks could be well-indexed to the standard data of the hexagonal phase of α-Fe_2O_3 (JCPDS 33-0664) with a space group of R3c and structural parameters of a = b =5.038 Å, c = 13.772Å. This implies that high purity α-Fe_2O_3 can be obtained by only adjusting the aging time in the presence of urea. The strong and sharp peaks indicated that the as-prepared products were highly crystalline in spite of no subsequent >80 °C high temperature treatment, which is just one of the many advantages when using our method.

The crystalline phase transformations characteristics are consistent with results previously reported. Hydrolysis of $FeCl_3$ to produce β-FeOOH then α-Fe_2O_3 had been investigated by many groups as a model system for a better understanding of the formation of iron oxides [31-34, 36, 38-39]. In our reaction system, the process produced β-FeOOH and α-Fe_2O_3 by hydrolysis of $FeCl_3$ can be described as follows:

$$FeCl_3 \rightarrow Fe(OH)_3 \rightarrow \beta\text{ - }FeOOH \rightarrow \alpha\text{ - }Fe_2O_3$$

That is, amorphous $Fe(OH)_3$ colloidal particles were formed and developed thought hydrolysis of $FeCl_3$ at 100℃. Then nucleation and growth of β-FeOOH was accomplished based on $Fe(OH)_3$ colloidal particles. β-FeOOH is a metastable structure. So the most thermodynamically stable α-Fe_2O_3 was finally synthesized when the aging time was long enough. Although the amount of urea was large variations in experiment, final products were all α-Fe_2O_3 after 12h aging (as shown in

Fig.1b). This implied that the phase transition rule from β-FeOOH to α-Fe_2O_3 depended on aging time and was independent of the amount of urea when there was urea.

To the best of our knowledge, there are two viewpoints about the transformation mechanisms from β-FeOOH to α-Fe_2O_3, the aggregation process of preformed primary particles and dissolution-recrystallization process [40-43]. Thought tracking and analyzing on the change trend of structures, we found that products were meta-stable β-FeOOH in initial stage. If given the time of rearranging $Fe^{3+}$and O^{2-}, more stable α-Fe_2O_3 had the chance to achieve nucleation and growth. So meta-stable β-FeOOH existed along with stable α-Fe_2O_3 in intermediate steps, during which the supersaturation for β-FeOOH decreased and β-FeOOH dissolved to maintain a state of equilibrium. It could thus be concluded that phase transformation from β-FeOOH to α-Fe_2O_3 was implemented by dissolution of unstable β-FeOOH phase and reprecipitation of the more stable α-Fe_2O_3 phase in our reaction system. But combined with the SEM results below showing, we consider that the dissolution re-crystallization process was confined to primary particles. Then, by aggregating each other, primary particles constructed larger size final products.

According to the Debye-Scherrer formula, the crystallite size of α-Fe_2O_3 (0.125mol L^{-1} urea)for (104) and (110) faces were 16.9nm and 13.5nm respectively, which implied that the primary particles or building blocks of α-Fe_2O_3 are nearly spherical with nano size.

The typical SEM images of the products obtained in the presence of urea for various aging times were showed in Fig. 2a, 2b and 2c. It could be seen that the morpholohy of products obtained via various aging time was different. The products were mainly composed of rod-like particles when aging time is shorter. As time went on, products with mulberry-like morphology appeared and increased gradually. When the aging time was long enough, products had uniform mulberry-like morphology. Compared with the XRD as shown in Fig. 1a, it could illustrate that the products morphologies were related to crystal structure. The rod-like products were tetragonal β-FeOOH and mulberry-like products were hexagonal α-Fe_2O_3 respectively. Besides,

the entire structures of produces were built of many smaller particles with nano-size. These nanoparticles connected to each other to form hierarchical rod-like or mulberry-like nanostructures, which is in agreement with the previous result of XRD computation about primary particles. This also indicated that both rod-like β-FeOOH and mulberry-like α-Fe_2O_3 were formed by aggregating of primary particles. On the other hand, aggregation mode of primary particles was closely related to its phase structure as shown in Fig.1a. Figure 2d showed the transmission electron microscopy (TEM) image of mulberry-like α-Fe_2O_3, demonstrating a nanostructure by aggregating of primary particles. The HRTEM image obtained from mulberry-like α-Fe_2O_3 shown in Fig. 2e indicated that a lattice spacing of 0.25 nm for the (110) planes clearly identified the α-Fe_2O_3 particles [44].The corresponding SAED pattern in the inset Figure revealed the polycrystallinity of the α-Fe_2O_3 nanostructure.

As compared with the control groups, above results also showed that the role of urea are not only the homogeneous precipitant agent in the conventional sense reported in literature [45]. This is because the $Fe(OH)_3$ nucleation or colloidal particles had been formed before urea was added to the system. Urea should have certain effect on forming, crystallizing and controlling morphology of products, as we shall discuss below.

Based on analysis of experimental phenomena and results, we considered that else role of urea was twofold, to coagulate fine colloid grains and to control aggregation of the primary particles. Our reaction system was weak acid solution with pH 4 -5. The decomposition products of urea are mainly ammoniums in this medium [46]. Ammoniums obtained from urea decomposing could be adsorbed on the surface of $Fe(OH)_3$ colloidal particles by hydrogen bonds and/or electrostatic interactions with surface hydroxyl. These led to colloidal particles sedimentate but inhibited the unrestricted growth of the particles. So the primary particles or building blocks of final products were uniform in nano-size. The second role of urea was to control aggregation mode between primary nanoparticles. These assigned ammoniums got close each other to aggregate primary particles into larger-size samples through hydrogen bond or other non - covalent interaction. Ammoniums adsorbed on the

surface were distributed spherical symmetrically when the coated particles were amorphous $Fe(OH)_3$. In this state, the colloidal particles aggregated with no dominant direction. When β-FeOOH was transformed, ammoniums were preferentially adsorbed in some directions, for instance, parallel or perpendicular to the some crystal faces because of uneven distribution of surface hydroxyl with tetragonal structure [31, 36]. As a result, the coated primary particles tend to oriented attachment to form hierarchical rod-like products. In the dissolution re-crystallization process from β-FeOOH to α-Fe_2O_3, the selective adsorption of ammoniums decreased. Ammoniums tended to spherically symmetric distribution in the surface of primary particles because of uniform distribution of surface hydroxyl in hexagonal structure of α-Fe_2O_3. So the aggregation way of primary particles was changed fall in between $Fe(OH)_3$ and β-FeOOH. As a result, α-Fe_2O_3 with hierarchical mulberry-like morphology was obtained. That is why we consider that phase transforming process from β-FeOOH to α-Fe_2O_3 was preferentially confined to primary particles. Scheme 2 showed the schematic of the role of urea. However, whether the rod-like β-FeOOH or mulberry-like α-Fe_2O_3, there were both limited aggregation. When the aggregation reached a balance the size and morphology of the final products could be fixed. The experimental results showed that equalization points would be controlled by some process conditions, including iron source concentration, pH value, aging time and so on.

Nitrogen adsorption–desorption isotherms of the rod-like β-FeOOH (obtained by 2h aging) and mulberry-like α-Fe_2O_3 (obtained by 8h and 12h aging respectively) were depicted in Fig. 3. All the isotherms the samples can be classified as type IV isotherms characteristic of mesoporous materials. The corresponding pore size distribution curves (the inset in Fig. 3) could illustrate the pores with a center about 16 nm for α-Fe_2O_3 and about 5 nm for β-FeOOH respectively. Combining with the results of SEM, we preliminary judged that these pores were likely due to the void space of nanoparticles aggregation. Different products gathered in different ways and aggregation degree. These iron oxides with hierarchical structure and abundant pore might have a wide range of applications in adsorption, catalysis and other fields.

The SEM images of α-Fe_2O_3/PS obtained by adding polystyrene spheres (PS) to reaction system were showed in Fig. 2f. The photo- degradation activity of α-Fe_2O_3/PS was evaluated toward methylene blue under sunlight irradiation. From Fig. 4, we could clearly see that about 98.2% of methylene blue was degraded after sunlight irradiation for 2.5 h exhibiting better activity. The result is very benefit for more in-depth research in the future work in this area. Specifically, α-Fe_2O_3/PS could be readily separated by filtration or sedimentation after reaction because of their nano-/micro hierarchical architectures. In addition, stability is very important for recycling of catalysts in practical applications. To prove the possibility of recyclability of α-Fe_2O_3/PS, cycle experiment was performed. From Fig. 5, we could clearly see that the ratio of photo-degradation was remained approximately constant after reused for 3 times. So the recyclability of α-Fe_2O_3/PS is possible and its stability in treating organic contaminated water is satisfactory. Results also showed considerable loss of activity in successive more times runs. It may be due to the reduce of the activity sites of produce surface and agglomeration of particles with increase of the number of recycling, which caused decreased of the degradation efficiency of methylene blue. Further exploring and developing are needed in our future researches.

3.2 The effect of saccharides on the structure and morphology of the products

Saccharide is frequently used as organic substrates in biomimetic synthesis of inorganic materials because they have abundant functional groups and strong biological effects. Especially it is important to study the role of saccharides in the formation process of iron oxide for understanding the geochemical behavior of iron mineral phases. Numerous mechanisms for the adsorption of saccharides onto iron oxides had been proposed. Hydrogen bonding, electrostatic interactions, hydrophobic interactions and surface complex had been the favoured mechanism [47-48].

Firstly, the effects of adding amount of glucose on the formation and phase transformation process of iron oxides were studied and analyzed. As shown in Fig.6, when the amount of added glucose is 1- 20mg/ml, as the aging time extended, tetragonal β-FeOOH phase was obtained firstly and transformed finally to more stable α-Fe_2O_3, which is in agreement with the results got in the absence of glucose. When

the amount of glucose exceeded 50mg/ml, as-obtained products always were β-FeOOH and no longer to translate α-Fe_2O_3 even if aging time extended over 12 h. The significance of this result lay in adding the right amount of glucose to obtain easily well-crystallized metastable state β-FeOOH. The experiment result in the hydrolysis system of $FeCl_3$ was seldom reported.

Fig. 7 showed the morphology of the as-obtained α-Fe_2O_3 (Fig. 7a) and β-FeOOH (Fig. 7b) when adding glucose 2mg/ml and 50mg/ml respectively. Compared with the results of XRD, it could see that the morphology of β-FeOOH was raft-like in presence of glucose. That is, nano-particles firstly aggregated to nano-rod and subsequently the latter gathered into raft-like in side-by-side.

Based the analysis on the experimental process and results, we believed that the main reason of adding glucose to change the structure and morphology of products was the role of the hydroxyl of glucose molecules. There should been the relatively strong interaction between these hydroxyl and those on the surface of primary particles. On the other hand, the hydroxyl-hydroxyl hydrogen bonds were involved in the aggregation between the primary particles. A higher glucose content might be formed a dense surface protective due to the interactions between the hydroxyl groups of glucose and those on the surface of primary particles, which could not only avoid growth abnormally or conglomeration of particles and also prevent the dissolution of β-FeOOH and rearrangement of structure. Thereby the phase transformation from the metastable β-FeOOH to more stabile α-Fe_2O_3 structure was inhibited. This finding opens up new vistas for synthesis of special morphology metastable β-FeOOH in mild conditions. Besides, because of the existence of relatively strong hydrogen bonds combined between glucose molecules and surface of particles, primary particles aggregated firstly to rod and subsequently gathered to raft-like in side-by-side.

The structure and morphology of products were investigated when adding starch and ganoderan to the reaction system. Results indicated that: (1) when adding starch, the phase transformation characteristics of the products were similar to that in presence of glucose. In other words, metastable β-FeOOH phase could be stabilized when the content of starch was relatively high (no less than 20mg/ml). But with

ganoderma polysaccharides amount of 1-15mg /ml we found no evidence to support the phase transformation from β-FeOOH to α-Fe_2O_3. This means that the polysaccharide have an advantage over simple sugars in stable β-FeOOH phase structure. This experimental result is very significant, indicating that the polysaccharide has a stabilizing effect for metastable phase β-FeOOH in our so mild system, which has not been reported. (2) It could be seen from Fig. 8a that the morphology of β-FeOOH obtained adding starch was needle-like but difference from rod-like that obtained in presence of glucose. Existence of ganoderma polysaccharide, the morphology of the product was peculiar pine needle-like hierarchical structure (Fig. 8b). The first layer consisted of nanoparticles with diameter of about 30nm. The nanorods with length of about 500nm were an integral component of the second layer, and the third layer was composed of β-FeOOH pine needles.

The formation of these novel morphologies could understand according to the structure characteristics of polysaccharide molecules and interaction between these molecules and iron oxides. We suggested that the effect of starch included three aspects. First, hydroxyl groups in the starch chain might react with hydroxyl groups on the surface of the primary particles [47-48]. When $FeCl_3$ saturated solution were dripped dropwise into the boiling starch solution, the reaction took place. These functional groups provided initial reaction sites, which resulted in a series of separate β-FeOOH crystal nucleus along the polysaccharide molecules. Second, chain structure of the starch played a template or a support role. β-FeOOH crystal nucleus grew on the starch chains and aggregated along the chain, eventually forming a relatively orderly long needle structure. Thirdly, starch would have a coating effect on iron oxide. Especially when the levels of starch were higher, the hydrogen bonds between the starch molecules were enhanced and solubility reduced causing gelation. In this case, the starch gel coated the surface of iron oxide particles to prevent the agglomeration between the iron oxide particles and exchange other inorganic components with liquid phase, thereby inhibiting the phase transformation from β-FeOOH to α-Fe_2O_3.

Ganoderan is mainly composed of β-glucan and other polysaccharides. Its

configuration is the form of a triple helix chains structure supported by the hydrogen bonds between the spiral layers, which are similar to the three-dimensional configuration of DNA. The role of the ganoderan was similar to starch in the formation of iron oxides. But unlike this, due to its three-dimensional helical configuration, ganoderan could induce the formation of products with pine needle-like morphology. In conclusion, when polysaccharides existed, morphology of products was the combination of structure of polysaccharides and interaction between the polysaccharides with iron oxides.

Scheme 3 showed the schematic of forming iron oxides with different morphologies discussed above. The main contribution to the synthesis of iron oxide is: (1) α-Fe_2O_3 and β-FeOOH with excellent crystallinity and uniform morphology can be obtained under mild green crystallization conditions; (2) The presence of polysaccharides was favorable to forming metastable β-FeOOH. The analysis on the procedure and mechanism may provide theoretical guides for the studies of iron oxides.

Nitrogen adsorption–desorption isotherms of three β-FeOOH obtained in presence of Glucose, starch and ganoderan respectively were depicted in Fig. 9, which all were classified as type IV isotherms characteristic of mesoporous materials. Combining with the results of SEM, we could preliminary judge that these pores were likely due to the void space of nanoparticles aggregation. As shown in Table 1, the surface areas were 125.42m^2/g for raft-like β-FeOOH(S1), 157.97 m^2/g for needle-like β-FeOOH(S2), and 193.85 m^2/g for pine needle-like β-FeOOH(S3), respectively. The data in the table illustrated as-obtained β-FeOOH has high specific surface area, pore volume and well- developed unique porous structure, which is the contribution of hierarchical nanostructures and may be widely used as adsorbent and photo-catalysts to treat wastewater.

Figure 10 showed the time-dependent degradation ratio of methycene blue under sunlight using the three different morphologie β-FeOOH S1, S2, S3 as photo-catalysts. From the degradation ratio, we could see that the relative photo-catalytic activity of

the catalysts decreased in the order of S3 > S2 > S1. The result accords with the specific surface area of products. The high specific surface area and abundant porous structures are the contribution of hierarchical nanostructures, which are the important factors of excellent photo-degradation activity.

4. Conclusion

In summary, we developed a facile, low-temperature, and environmentally friendly process for the fabrication of hierarchical nanostructured α-Fe_2O_3 and β-FeOOH. These iron oxides were constituted through aggregation of primary nanoparticles resulting in the interesting hierarchical morphology, the controlled crystal phase structures, higher stability and promising catalytic activity for degradation of methylene blue under sunlight irradiation. The results proved that the urea made control action on the crystallization and morphology of iron oxides. The saccharide played an important role in the controlling products morphology and stabilizing β-FeOOH crystalline phase. In essence, this method is a biomimetica mineralization process involved organics and products are a class of the organic-inorganic hybrid materials. We think that these hierarchical nanostructure iron oxides may have great applications in photo-catalysis, catalysis, separation and purification processes. This study can provide an example for better understanding the formation mechanism of other inorganic hierarchical materials in the presence of natural organic matter. We believe that the present work will open up to systematically explore ways to fabricate hierarchical structures and thus find use in a variety of applications.

Acknowledgments

This work was supported by NSFC (No. 21477032) and Hebei Natural Science Foundation (No. B2014205085).

References

[1] S. W. Cao, Y. J. Zhu, J. Phys. Chem. C., 2008, 112, 6253.

[2] Q. Y. Hao, S. Liu, X. M. Yin, Z. F. Du, M. Zhang, L. M. Li, Y. G. Wang, T. H. Wang, Q. H. Li, CrystEngComm., 2011, 13, 806.

[3] J. S. Xu, Y. J. Zhu, CrystEngComm., 2011, 13, 5162.

[4] C. Zhang, Z. Mo, C. D. Jiang, P. Zhang, R. B. Guo, CrystEngComm., 2013, 15, 6546.

[5] D. Z. Zhu, J. Zhang, J. M. Song, H. S. Wang, Z. Yu, Y. H. Shen, A. J. Xie, Appl. Surf. Sci., 2013, 284, 855.

[6] J. J. Zhang, Y. L. Chen, Y. F. Sun, T. Huang A. S. Yu, RSC Adv., 2013, 3, 20639.

[7] L. S. Zhong, J. S. Hu, H. P. Liang, A. M. Cao, W. G. Song, L. J. Wan, Adv. Mater., 2006, 18, 2426.

[8] H. U. Lee, S. C. Lee, Y. C. Lee, S. Vrtnik, C. Kim, S. G. Lee, Y. B. Lee, B. Nam, J. W. Lee, S. Y. Park, S. M. Lee, J. Lee, J. Hazard. Mater., 2013, 262, 130.

[9] J. G. Yu, X. X. Yu, B. B. Huang, X. Y. Zhang, Y. Dai, Cryst. Growth Des., 2009, 3, 1474.

[10] C. C. Wan, J. Li, ACS Sustainable Chem. Eng., 2015, 3, 2142.

[11] M. M Rahman, A. Jamal, S. B. Khan, M. Faisal, J. Nanopart Res., 2011, 13, 3789.

[12] A. Mouradzadegun, L. Ma'mani, M. Mahdavi, Z. Rashid, S. dianat, RSC Adv., 2015, Accepted Manuscript

[13] M. M. Rahman, S. B. Khan, M. Faisal, A. M. Asiri, M. A. Tariq, Electrochimica Acta., 2012, 75, 164.

[14] M. M. Rahman, A. Jamal, S. B. Khan, M. Faisa, Superlattices and Microstructures, 2011, 50, 369

[15] M. Charles, J. R. Flynn, Chem. Rev., 1984, 84, 31.

[16] E. C. Spencer, N. L. Ross, R. E. Olsen, B. Y. Huang, A. I. Kolesnikov, B. F. Woodfield, J. Phys. Chem. C, 2015, 119 (17), 9609.

[17] A. D. Wheeler, G. Wang, Y. H. Ling, Y. Li, J. Z. Zhang, Energy Environ. Sci., 2012, 5, 6682.

[18] G. Liu, Q. Deng, H. Q. Wang, D. H. L. Ng, M. G. Kong, W. P. Cai, G. Z. Wang, J. Mater. Chem., 2012, 22, 9704.

[19] H. J. Cui, J. K. Cai, J. W. Shi, B. L. Yuan, C. L. Ai, M. L. Fu, RSC Adv., 2014, 4, 10176.

[20] Y. Jiao, Y. Liu, F. Y. Qu, X. Wu, CrystEngComm., 2014, 16, 575.

[21] E. T. Liu, H. P. Zhao, H. Li, G. F. Li, Y. L. Liu, R. Chen, New J. Chem., 2014, 38, 2911.

[22] Z. H. Wei, R. G. Xing, X. Zhang, S. Liu, H. H. Yu, P. C. Li, ACS Appl. Mater. Interfaces., 2013, 5, 598.

[23] L. L. Wang, T. Fei, Z. Lou, T. Zhang, ACS Appl. Mater. Interfaces., 2011, 3, 4689.

[24] C. Y. Cao, J. Qu, W. S. Yan, J. F. Zhu, Z. Y. Wu, W. G. Song, Langmuir., 2012, 28, 4573.

[25] R. Kant, D. Kumar, V. Dutta, RSC Adv., 2015, 5, 52945.

[26] C. Hao, F. Feng, X. H. Wang, M. Zhou, Y. T. Zhao, C. W. Ge, K. Wang, RSC Adv., 2015, 5, 21161.

[27] X. L. Cheng, J. S. Jiang, M. Hu, G. Y. Mao, F. X. Bu, C. C. Lin, Y. Zeng Q. H. Zhang, CrystEngComm., 2012, 14, 7701.

[28] M. Muruganandham, R. Amutha, M. Sathish, T. S. Singh, R. P. S. Suri, M. Sillanpää, J. Phys. Chem. C., 2011, 115, 18164.

[29] W. F. Tan, Y. T. Yu, M. X. Wang, F. Liu, L. K. Koopal, Cryst. Growth Des., 2014, 14, 157.

[30] M. T. Klem, M. Y. T. Douglas, J. Mater. Chem., 2010, 65.

[31] X. Wang, X. Y. Chen, L. S. Gao, H. G. Zheng, M. R. Ji, C. M. Tang, T. Shen, Z. D. Zhang, J . Mater. Chem., 2004, 14, 905.

[32] N. K. Chaudhari, J. S. Yu, J. Phys. Chem. C., 2008, 112, 19957.

[33] M. Žic, M. Ristić, S. Musić, J. Alloys Compd., 2008, 464, 81.

[34] X. H. Rao, X. T. Su, C. Yang, J. D. Wang, X. P. Zhen, D. H. Ling, CrystEngComm., 2013, 15, 7250.

[35] S. Musić, S. Krehulaa, S. Popović, Mater. Lett., 2004, 58, 444.

[36] H. F. Shao, X. F. Qian, J. Yin, Z. K. Zhu, J. Solid State Chem., 2005, 178, 3130.

[37] M. Chowdhury, V. Fester, G. Kale, J. Cryst. Growth., 2014, 387, 57.

[38] J. K. Bailey, C. J. Brinker, M. L. Mecartney, J. Colloid Interface Sci., 1993, 157, 1.

[39] W. Wang, J. Y. Howe, B. H. Gu, J. Phys. Chem. C., 2008, 112, 9203.

[40] T. Sugimoto, A. Muramatsu, J.colloid Interface Sci., 1996, 184, 626.

[41] T. P. Almeida, M. W. Fay, Y. Zhu, P. D. Brown, Nanoscale., 2010, 2, 2390.

[42] M. Lin, H. R. Tan, J. P. Y. Tan, S. Q. Bai, J. Phys. Chem. C., 2013, 117, 11242.

[43] C. Frandsen, B. A. Legg, L. R. Comolli, H. Zhang, B. Gilbert, E. Johnsone, J. F. Banfield, CrystEngComm., 2014, 16, 1451.

[44] X. Jia, F. Yue, X. Chen, H. B. Pan, W. G. Liu, J. Y. Liu, RSC Adv., 2014, 4, 42899.

[45] M. O. M. P. Morales, C. J. Serna, J. Colloid Interface Sci., 1999, 212, 317.

[46] W. H. R. Shaw, J. J. Bordeaux, J. Am. Chem. Soc., 1955, 77, 4729.

[47] P. K. Weissenborn, L. J. Warren, J.G. Dunn, Colloids Surfaces A: Physicochem. Eng., 1995, 99, 11.

[48] E. Somsook, D. Hinsin, P. Buakhrong, R. Teanchai, N. Mophan, M. Pohmakotr, J. Shiowatana, Carbohydrate Polymers., 2005, 61, 281.

Captions for Figures:

Scheme 1 Schematic flow chart for the preparation of iron oxides by hydrolysis-aging method.

Figure 1 XRD patterns of the as-prepared iron oxides with changing of (a) aging time and (b) the amount of urea.

Figure 2 SEM and TEM images of the as-synthesized iron oxide at different aging time: (a) 2h, (b) 4h, (c) 8h, (d) TEM of α-Fe_2O_3, (e) HRTEM of α-Fe_2O_3 and (f) α-Fe_2O_3/PS.

Scheme 2 Schematic illustration for the effect of urea on aggregation mode of primary particles.

Figure 3 Nitrogen adsorption-desorption isotherms and pore size distribution (inset) of the as-prepared β-FeOOH and α-Fe_2O_3 with different aging time.

Figure 4 Time profiles of photo-catalytic degradation of methylene blue for α-Fe_2O_3/PS. The inset shows the PL spectra in the photocatalytic process.

Figure 5 The recycling of α-Fe_2O_3/PS for photodegradation of methylene blue.

Figure 6 XRD patterns of the as-prepared iron oxides in the presence of glucose with amount of (a)1mg/ml, (b) 2mg/ml, (c) 20mg/ml, and (d) 50mg/ml.

Figure 7 SEM images of the as-prepared iron oxide in the presence of glucose: (a) α-Fe_2O_3, (b) β-FeOOH.

Figure 8 SEM images of β-FeOOH in the presence of polysaccharide: (a) starch, (b) ganoderan.

Scheme 3 Schematic illustration of the formation and morphology of as-prepared hierarchical

nanostructures iron oxides under various conditions.

Figure 9 Nitrogen adsorption-desorption isotherms and pore size distribution (inset) of three kinds of β-FeOOH.

Figure 10 Time profiles of photo-catalytic degradation of methylene blue of three kinds of β-FeOOH.

Table 1 Physical characteristics of the as-prepared three kinds of β-FeOOH.

β-FeOOH sample	BET surface area (m^2 g^{-1})	Pore volume (cm^3 g^{-1})	BJH pore size (nm)
S1	125.42	0.263	9.55
S2	157.97	0.449	4.29
S3	193.85	0.725	9.70

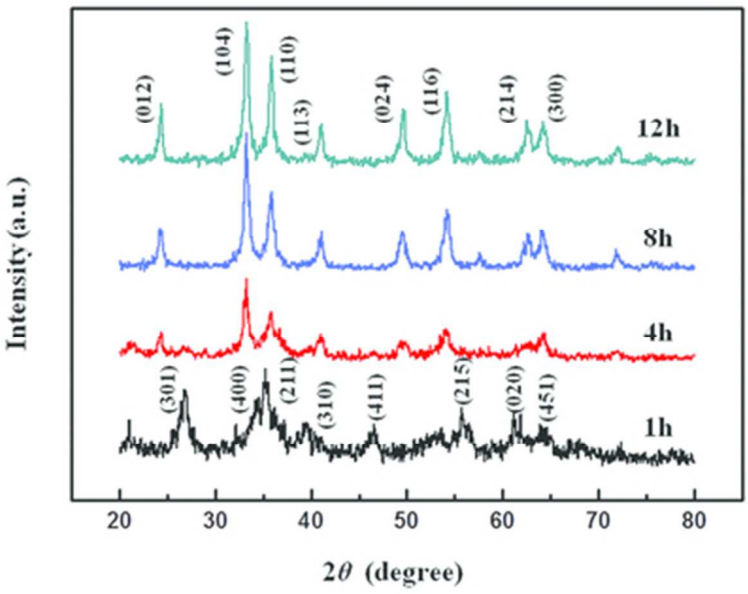

Figure 1 XRD patterns of the as-prepared iron oxides with changing of (a) aging time and (b) the amount of urea.
44x33mm (300 x 300 DPI)

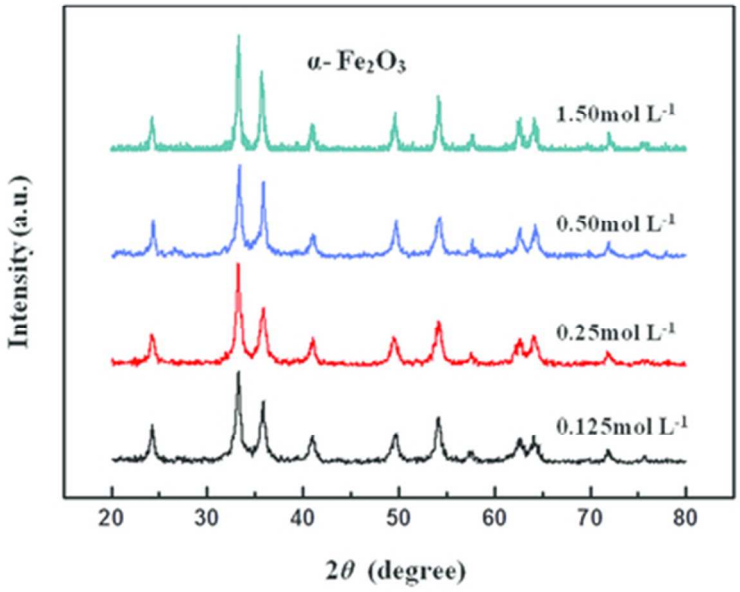

Figure 1 XRD patterns of the as-prepared iron oxides with changing of (a) aging time and (b) the amount of urea.
44x33mm (300 x 300 DPI)

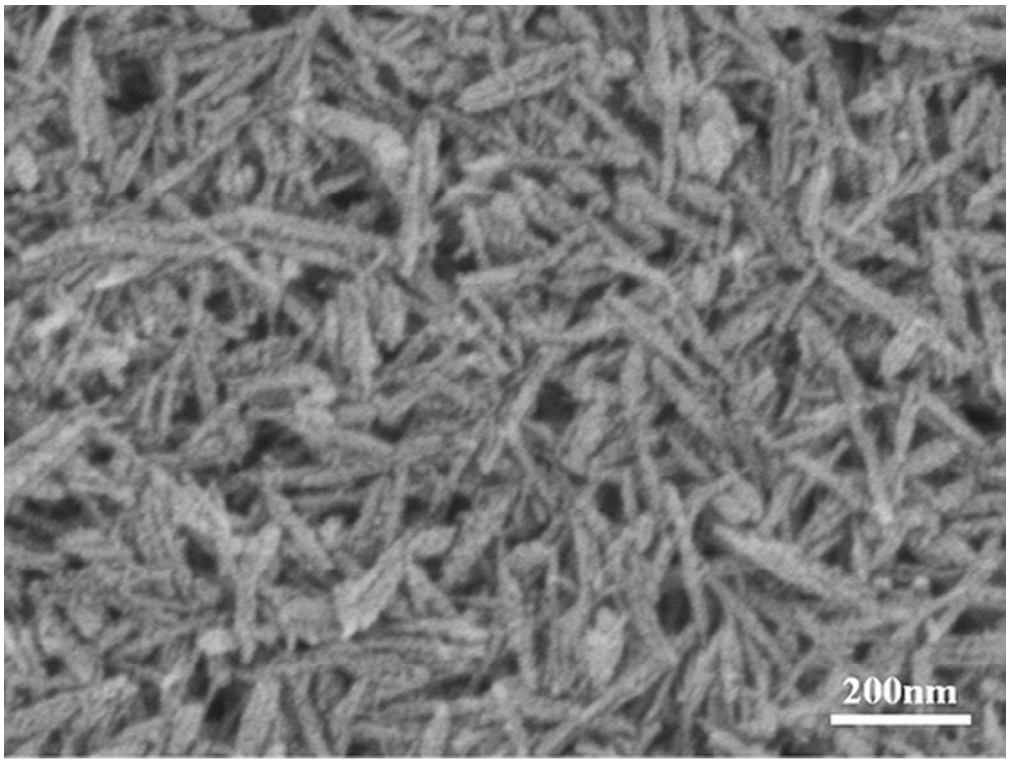

Figure 2 SEM and TEM images of the as-synthesized iron oxide at different aging time: (a) 2h, (b) 4h, (c) 8h, (d) TEM of α-Fe2O3, (e) HRTEM of α-Fe2O3 and (f) α-Fe2O3/PS.
45x33mm (300 x 300 DPI)

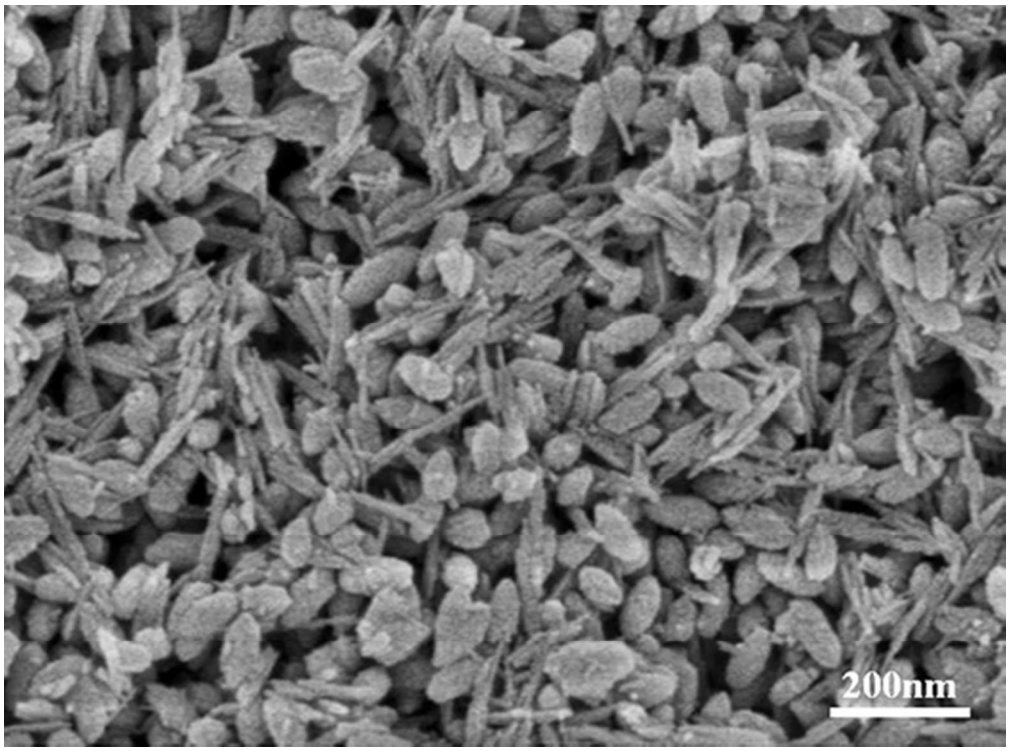

Figure 2 SEM and TEM images of the as-synthesized iron oxide at different aging time: (a) 2h, (b) 4h, (c) 8h, (d) TEM of α-Fe2O3, (e) HRTEM of α-Fe2O3 and (f) α-Fe2O3/PS.
44x32mm (300 x 300 DPI)

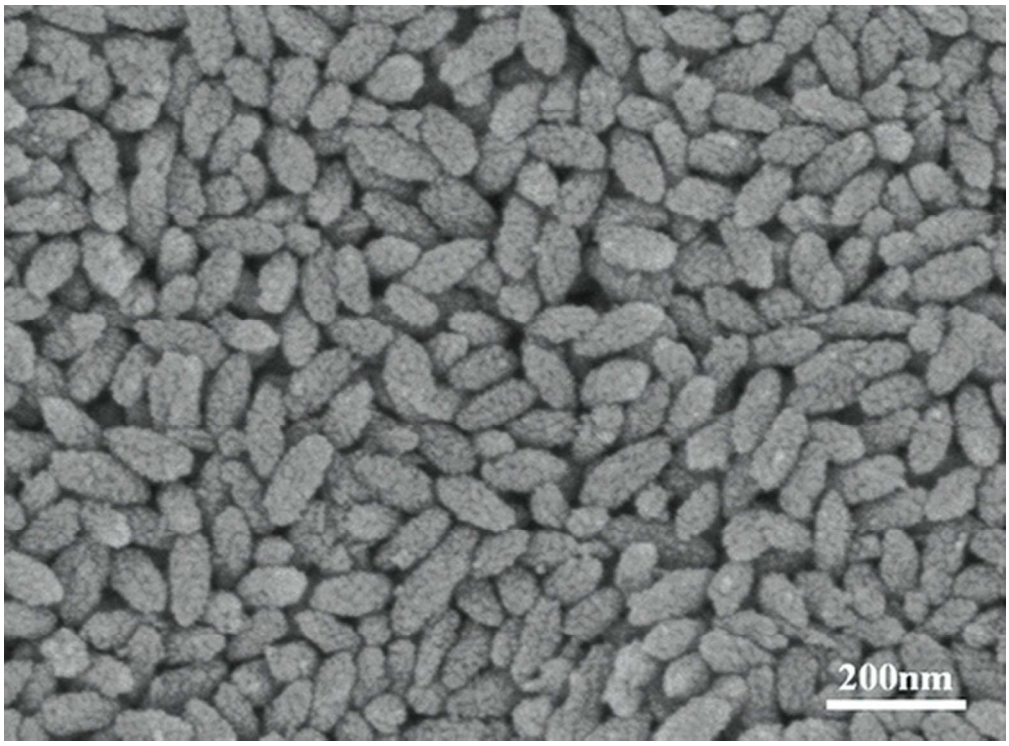

Figure 2 SEM and TEM images of the as-synthesized iron oxide at different aging time: (a) 2h, (b) 4h, (c) 8h, (d) TEM of α-Fe2O3, (e) HRTEM of α-Fe2O3 and (f) α-Fe2O3/PS.
44x32mm (300 x 300 DPI)

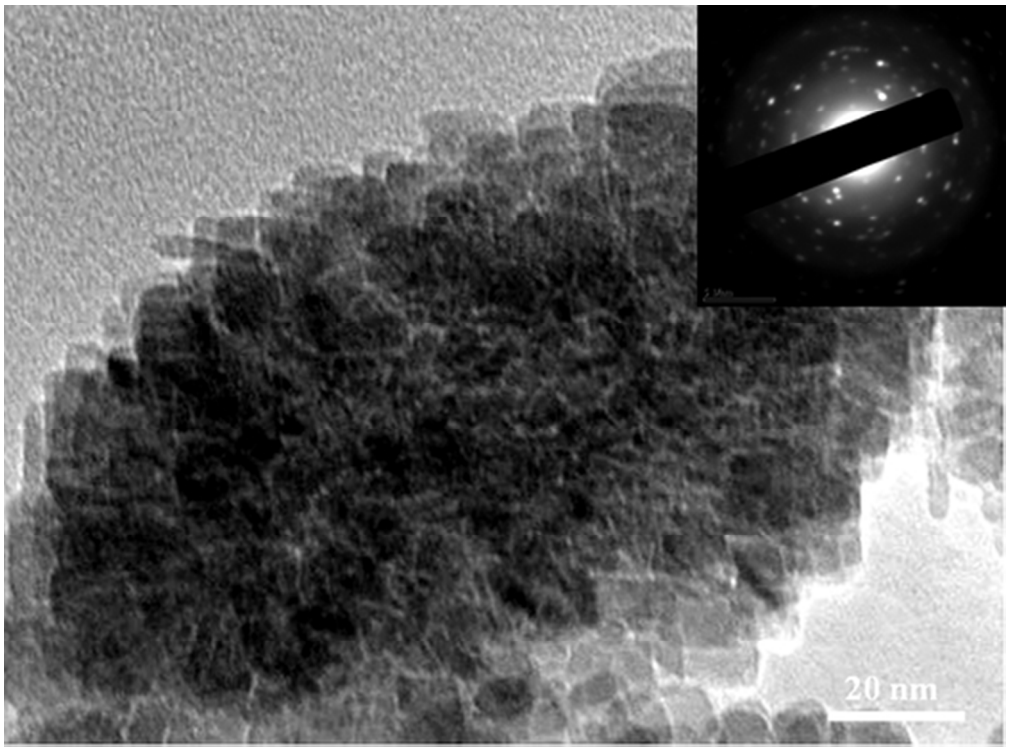

Figure 2 SEM and TEM images of the as-synthesized iron oxide at different aging time: (a) 2h, (b) 4h, (c) 8h, (d) TEM of α-Fe2O3, (e) HRTEM of α-Fe2O3 and (f) α-Fe2O3/PS.
44x32mm (300 x 300 DPI)

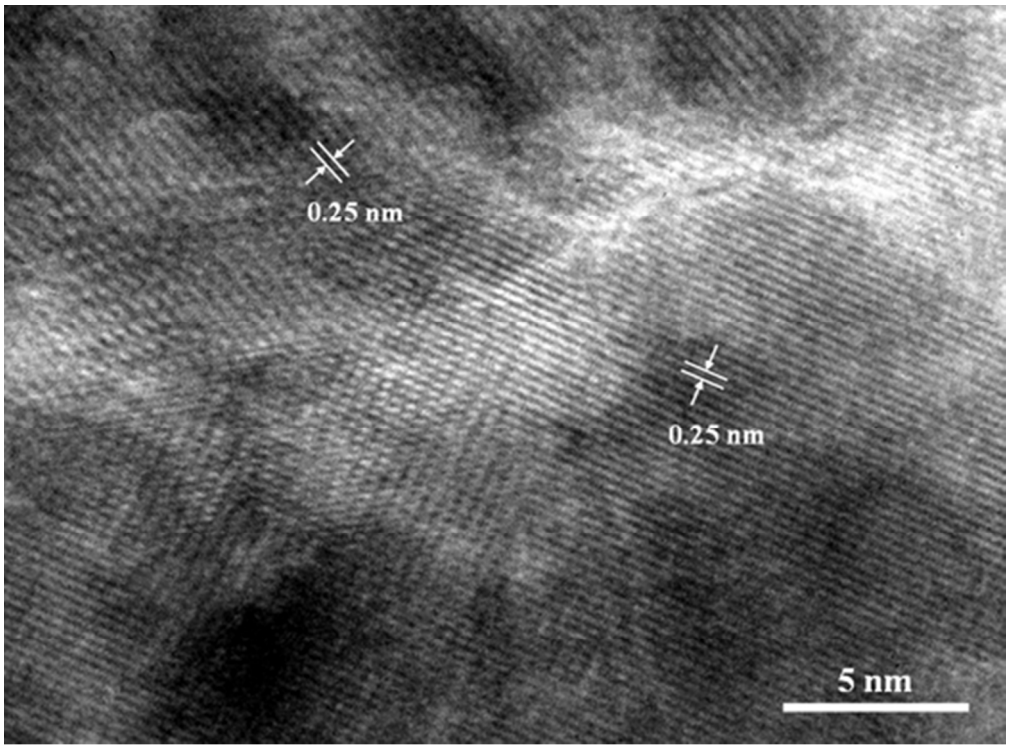

Figure 2 SEM and TEM images of the as-synthesized iron oxide at different aging time: (a) 2h, (b) 4h, (c) 8h, (d) TEM of α-Fe2O3, (e) HRTEM of α-Fe2O3 and (f) α-Fe2O3/PS.
44x32mm (300 x 300 DPI)

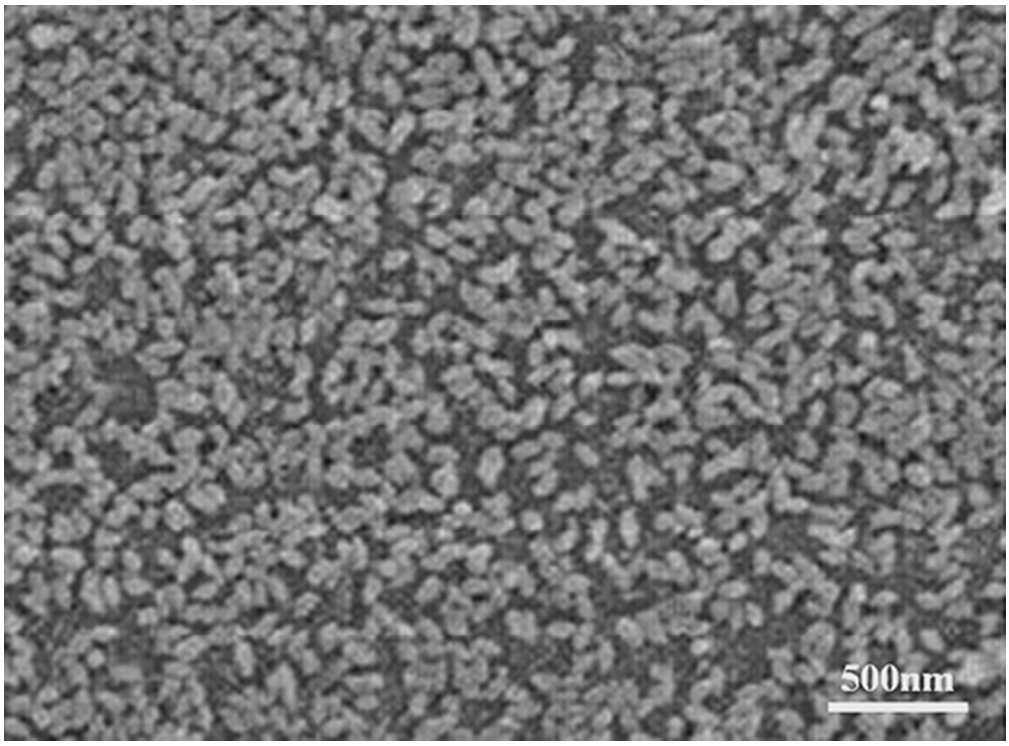

Figure 2 SEM and TEM images of the as-synthesized iron oxide at different aging time: (a) 2h, (b) 4h, (c) 8h, (d) TEM of α-Fe2O3, (e) HRTEM of α-Fe2O3 and (f) α-Fe2O3/PS.
44x32mm (300 x 300 DPI)

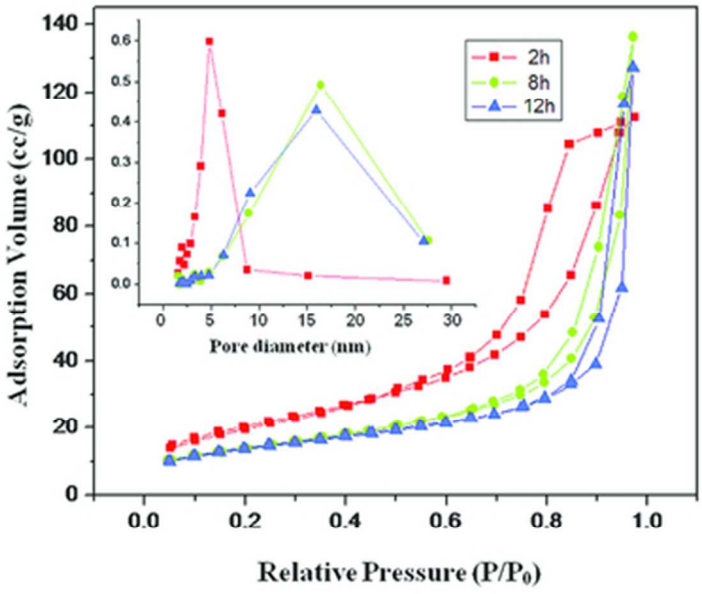

Figure 3 Nitrogen adsorption-desorption isotherms and pore size distribution (inset) of the as-prepared β-FeOOH and α-Fe2O3 with different aging time.
44x33mm (300 x 300 DPI)

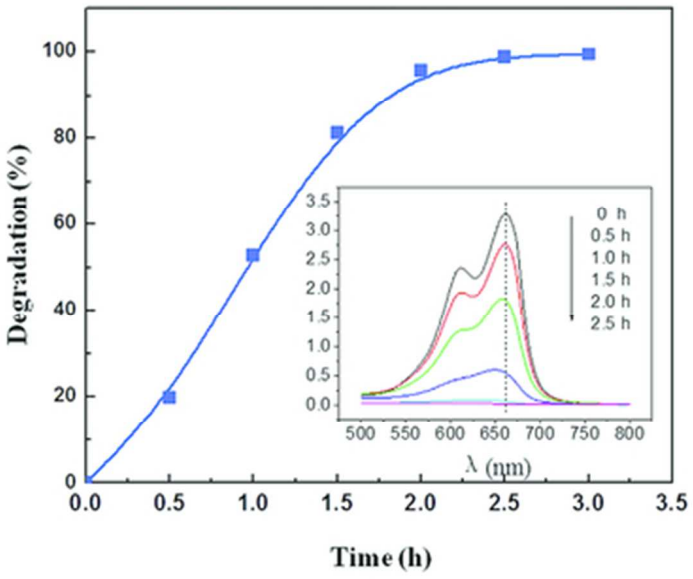

Figure 4 Time profiles of photo-catalytic degradation of methylene blue for α-Fe2O3/PS. The inset shows the PL spectra in the photocatalytic process.
44x33mm (300 x 300 DPI)

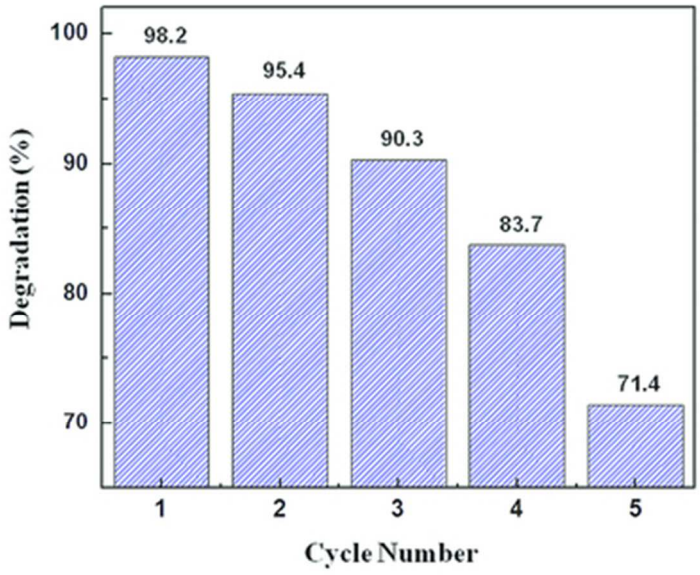

Figure 5 The recycling of α-Fe2O3/PS for photodegradation of methylene blue.
44x33mm (300 x 300 DPI)

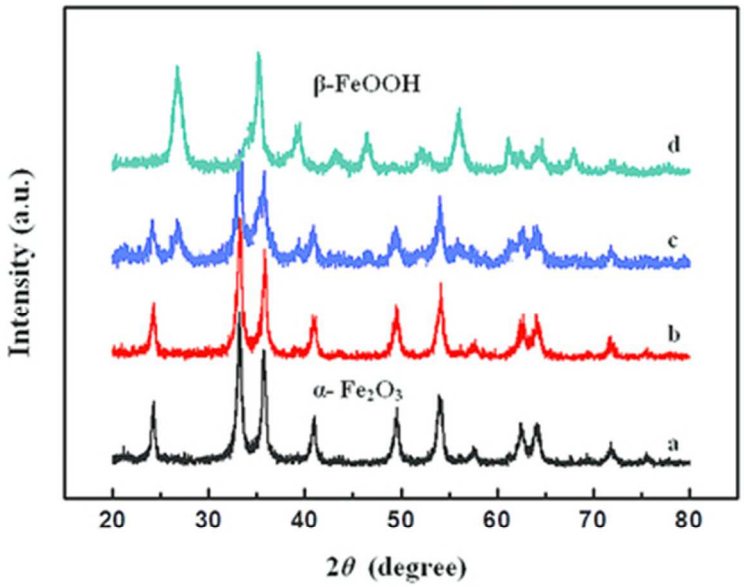

Figure 6 XRD patterns of the as-prepared iron oxides in the presence of glucose with amount of (a)1mg/ml, (b) 2mg/ml, (c) 20mg/ml, and (d) 50mg/ml.
44x33mm (300 x 300 DPI)

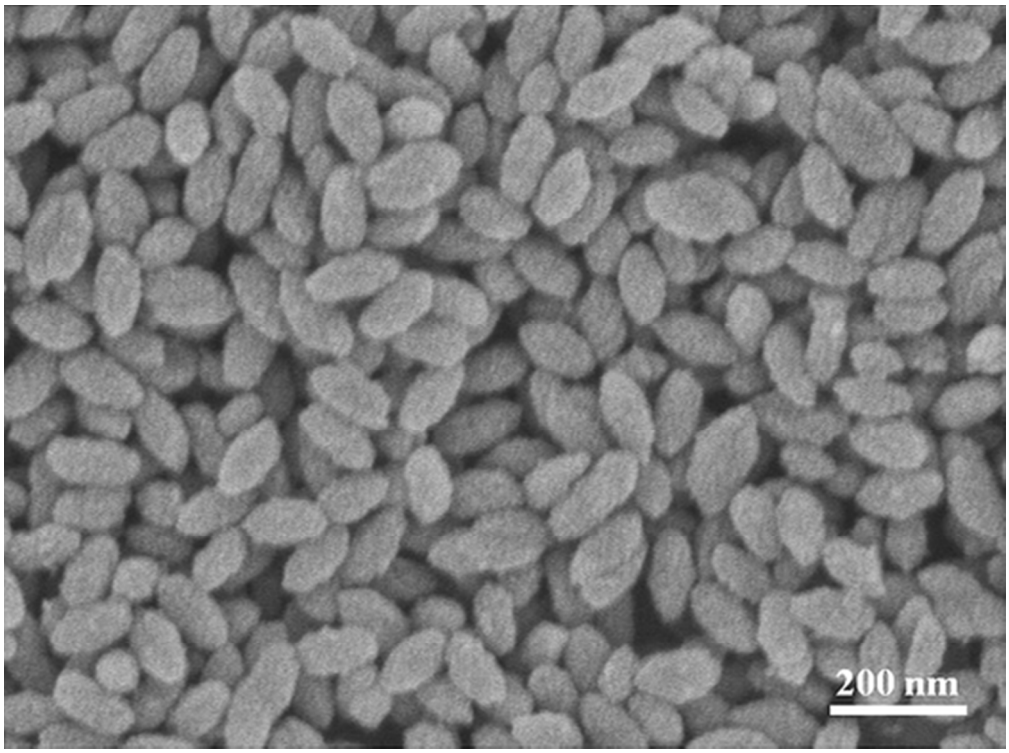

Figure 7 SEM images of the as-prepared iron oxide in the presence of glucose: (a) α-Fe2O3, (b) β-FeOOH.
44x33mm (300 x 300 DPI)

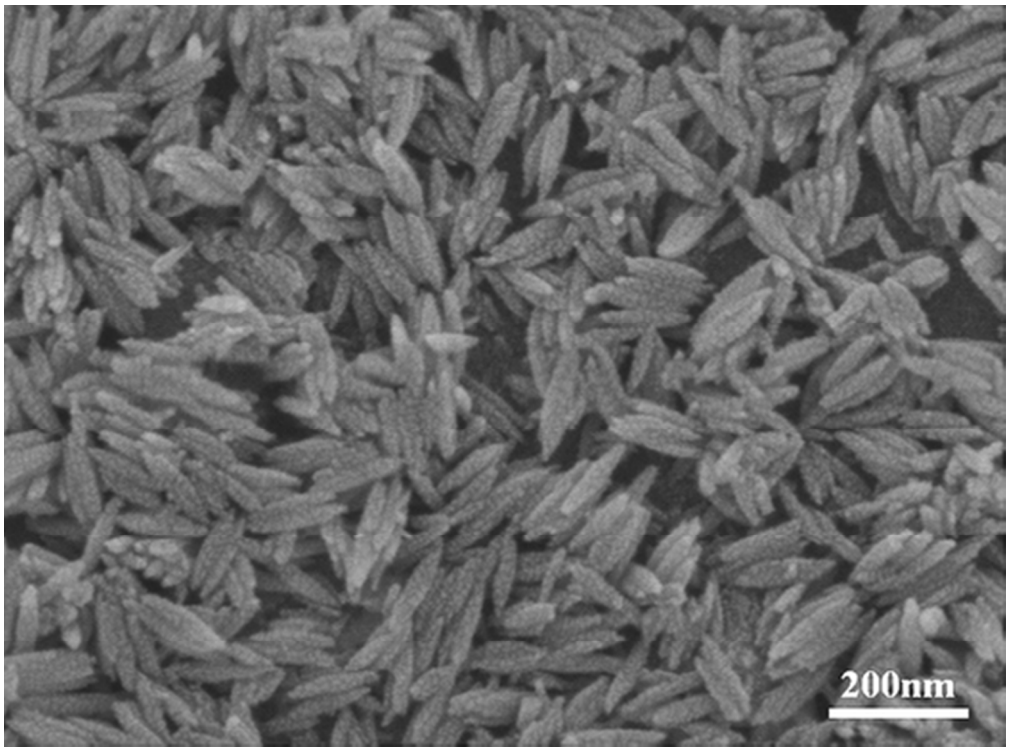

Figure 7 SEM images of the as-prepared iron oxide in the presence of glucose: (a) α-Fe2O3, (b) β-FeOOH.
44x32mm (300 x 300 DPI)

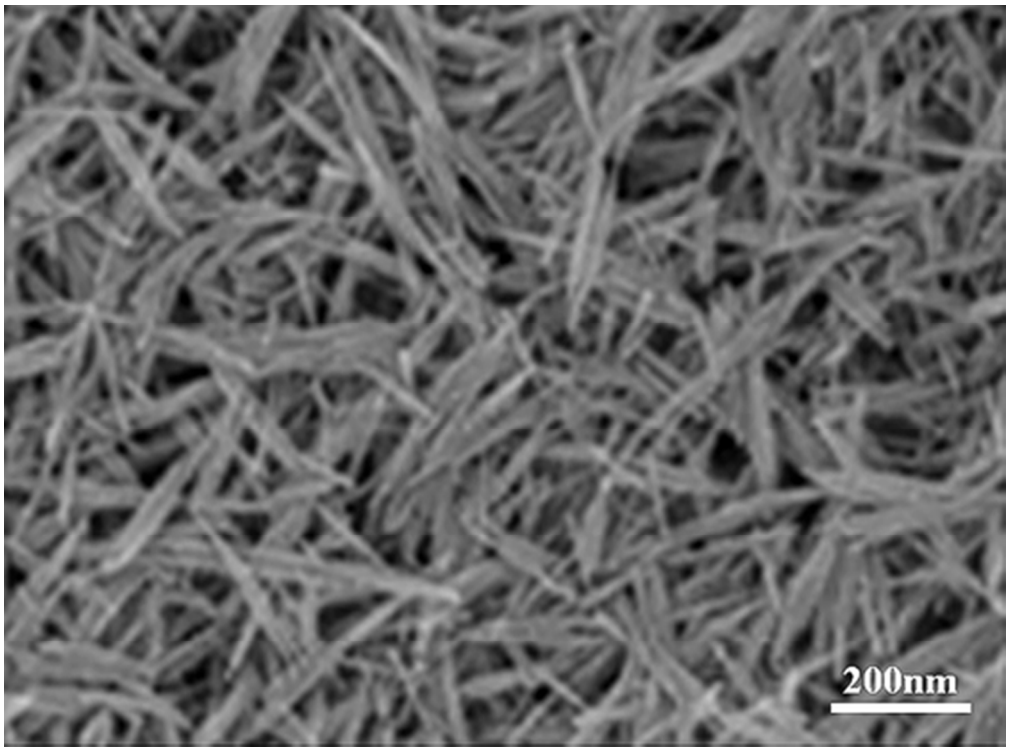

Figure 8 SEM images of β-FeOOH in the presence of polysaccharide: (a) starch, (b) ganoderan.
44x32mm (300 x 300 DPI)

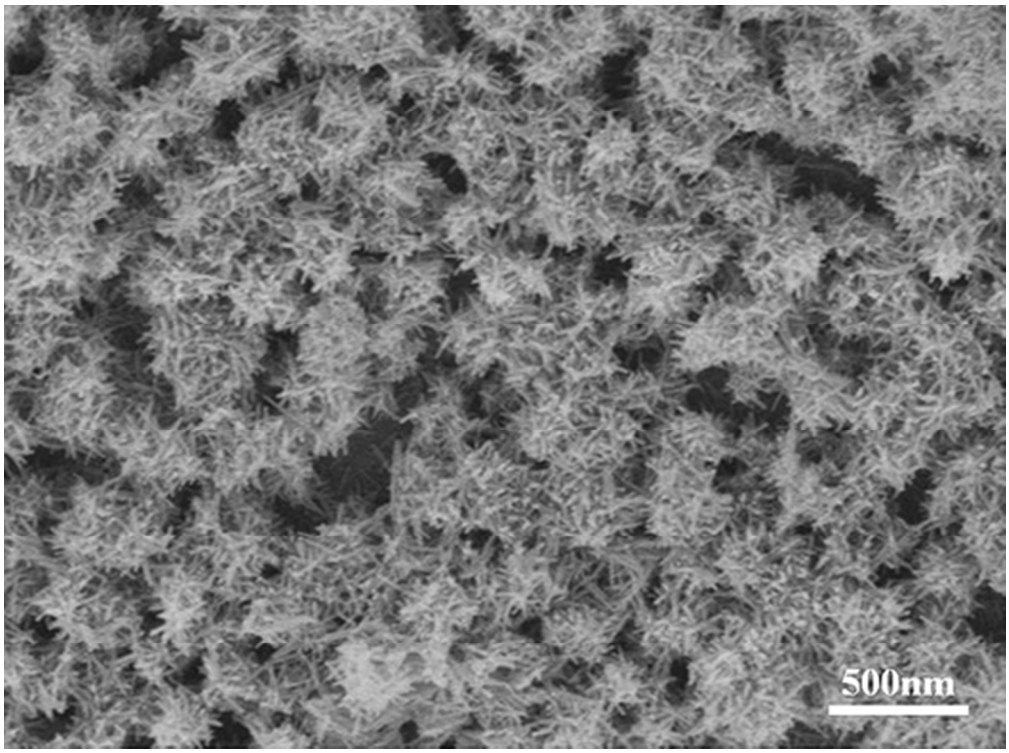

Figure 8 SEM images of β-FeOOH in the presence of polysaccharide: (a) starch, (b) ganoderan.
44x33mm (300 x 300 DPI)

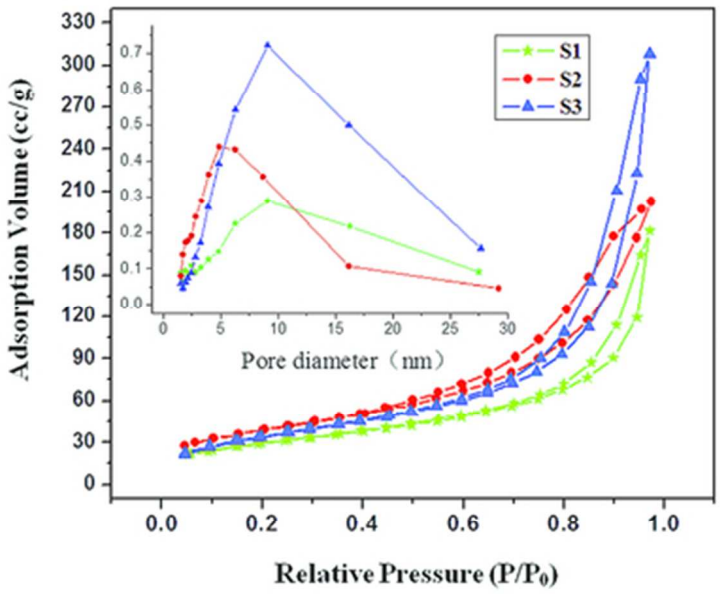

Figure 9 Nitrogen adsorption-desorption isotherms and pore size distribution (inset) of three kinds of β-FeOOH.
44x33mm (300 x 300 DPI)

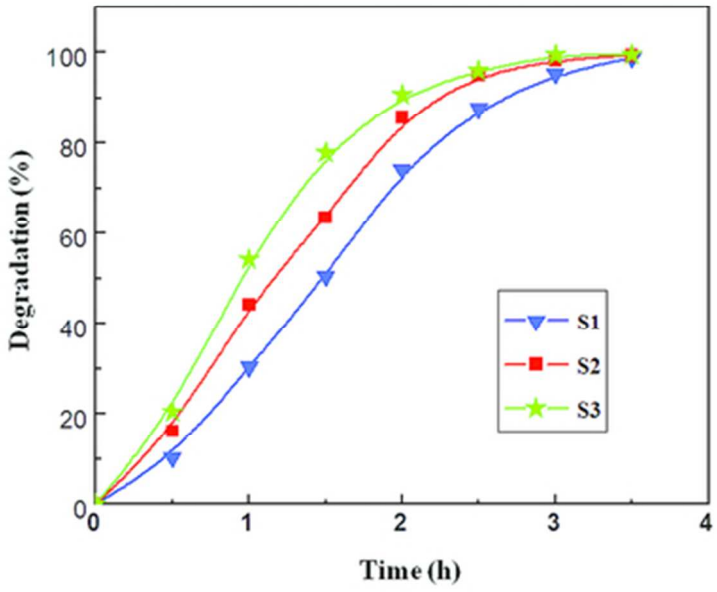

Figure 10 Time profiles of photo-catalytic degradation of methylene blue of three kinds of β-FeOOH.
44x33mm (300 x 300 DPI)

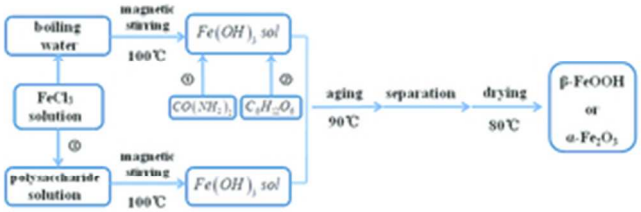

Scheme 1 Schematic flow chart for the preparation of iron oxides by hydrolysis-aging method.
29x14mm (300 x 300 DPI)

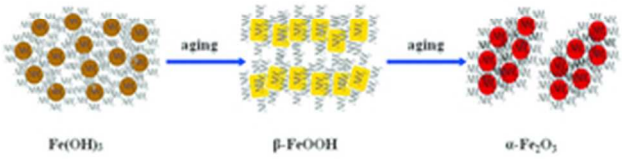

Scheme 2 Schematic illustration for the effect of urea on aggregation mode of primary particles.
29x14mm (300 x 300 DPI)

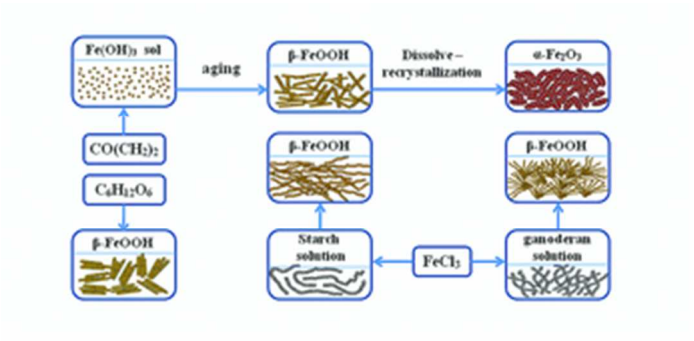

Scheme 3 Schematic illustration of the formation and morphology of as-prepared hierarchical nanostructures iron oxides under various conditions.
29x14mm (300 x 300 DPI)